Eur. Phys. J. E (2007)
DOI 10.1140/epje/i2006-10079-y

THE EUROPEAN PHYSICAL JOURNAL E

Diffusive Wave Spectroscopy of a random close packing of spheres

J. Crassous[a]

Groupe Matière Condensée et Matériaux UMR CNRS 6626, Université de Rennes1, Campus de Beaulieu, Bâtiment 11A, 35042 Rennes Cedex, France

Received 12 July 2006 and Received in final form 18 April 2007
Published online: 11 June 2007 –

Abstract. We are interested in the propagation of light in a random packing of dielectric spheres within the geometrical optics approximation. Numerical simulations are performed using a ray tracing algorithm. The effective refractive indexes and the transport mean free path are computed for different refractive indexes of spheres and intersticial media. The variations of the optical path length under small deformations of the spheres assembly are also computed and compared to the results of Diffusive Wave Spectroscopy experiments. Finally, we propose a measure of the transport mean free path and a Diffusive Wave Spectroscopy experiment on a packing of glass spheres. The results of those experiments agree with the predictions of this ray tracing approach.

PACS. 42.25.Dd Wave propagation in random media – 78.35.+c Brillouin and Rayleigh scattering; other light scattering – 81.05.Rm Porous materials; granular materials

1 Introduction

Deformations of granular media may occur at very different length scales ranging from the geophysical scale, down to the individual grain motion [1]. Getting experimental information on the motion of particles is a difficult task, not only due to this wide spread of scales, but also because the materials are currently opaque, leading experimentalists to use techniques which do not involve direct imaging. In order to get different kinds of information on the heterogeneity of the media [2] or on the dynamics of the granular media [3], the propagation and the scattering of acoustic waves traveling in those heterogeneous media may be used. Light scattering may also be used in order to get information on motions within granular media at the scale of the optical wavelength [4–8]. However the relationship between the evolution of the scattered light and the dynamics of a granular medium has not yet been considered in details in preceding studies. We discuss in this paper this relationship with the help of a numerical algorithm of ray tracing. In Section 2 we first present the ray tracing algorithm (2.1), discuss some geometrical properties of the rays (2.2), determine transport mean free paths as a function of the refractive indexes and we compare the results with some experimental values reported in the literature (2.3). In Section 3, we consider the deformations of the granular medium (3.1), and we compute the variations of the optical length induced by this deformation (3.2). The numerical results are then compared to a simplified analytical model (3.3). In Section 4, we present two experiments on a packing of glass spheres dispersed in air. First a transmission experiment (4.1) is presented, and the transport mean free path is measured. In Section 4.2 a Diffusive Wave Spectroscopy experiment on a packing submitted to thermal dilatation is done and compared to geometrical optics computations. We finish with concluding remarks and possible experiments in Section 5.

2 Diffusive transport of light

2.1 Numerical algorithm

For this study, I largely use the propagation of a light ray using a ray-tracing algorithm through a close random packing of identical spheres. The assembly of identical spheres of radius R is computed by the repetition of a $10R \times 10R \times 10R$ cube with periodic boundaries. I used for this the algorithm described by Jodrey *et al.* [9] for generating a packing with a solid fraction $\phi \approx 0.637$. Although the sphere packing is indeed periodical, no computed quantity keeps any trace of this periodicity. It was checked that the results were identical for a periodic assembly with a $5R \times 5R \times 5R$ elementary cube. The results of the simulation are also similar to a non-periodic configuration in a $200R \times 200R \times 200R$ box generated by free fall of

[a] e-mail: jerome.crassous@univ-rennes1.fr

granular beads into a box. However, the density obtained with such an algorithm is significantly lower, and the numerical values of computed quantities like the mean free path are slightly different. For given refractive indexes of the sphere n_{int} and of the continuous medium n_{ext}, a ray is calculated according to Snell-Descartes laws of reflection and refraction. The ray is a succession of reflections and refractions, with probabilities given by the Fresnel formulas.

For this, we consider an electric field with a linear polarization along a unit vector $\mathbf{s}$. The components of $\mathbf{s}$ along the parallel ($\mathbf{e}_\parallel$) and perpendicular ($\mathbf{e}_\perp$) unit vectors with respect to the scattering plane are computed as $\mathbf{s} = A_\parallel \mathbf{e}_\parallel + A_\perp \mathbf{e}_\perp$. The probability p that a reflection occurs is then calculated as $p = r_\parallel^2 A_\parallel^2 + r_\perp^2 A_\perp^2$, where $r_\parallel$ and $r_\perp$ are the reflection coefficients for electric field parallel and perpendicular to the scattering plane given by Fresnel formulas. The choice of the scattering event, *i.e.* reflection or refraction is randomly done according to this probability. The next unit vector $\mathbf{s}'$ of the polarization after the scattering event is then calculated as

$$\mathbf{s}' = \frac{r_\parallel A_\parallel \mathbf{e}_\parallel + r_\perp A_\perp \mathbf{e}_\perp}{\| r_\parallel A_\parallel \mathbf{e}_\parallel + r_\perp A_\perp \mathbf{e}_\perp \|}\,, \tag{1}$$

if the scattering event is a reflection. If the scattering event is a refraction, reflection coefficients should be replaced by transmission coefficients in (1).

The results of the ray-tracing algorithm is checked in two different ways. First, the results are compared to the computation of the transmittance of the Christiansen filter made of glass beads of Hoffmann [10,11]. Secondly, a very dilute sample of water spheres is simulated, and intensity and polarizations of the multiples rainbows are compared to van de Hulst data [12]. In each case the comparisons with data are excellent.

2.2 Steps lengths

In this geometrical optics description of light propagation in a glass bead assembly, the photons follow a random walk consisting in scattering events which are either refractions or reflections. The directions of the photon before and after the scattering event are not independent, but fixed by Snell-Descartes laws, and thus constitute a persistent random walk. The walk consists in steps which are inside or outside the spheres. Due to the geometry of the sphere packing, the steps inside and outside the spheres are different and must be separated for the analysis.

Figure 1 shows the mean length for steps which are inside and outside the spheres. Those behaviors may be easily understood. We notice first that the average distance between two points uniformly distributed on a sphere is $4R/3$. Thus the mean length of the segment joining two successive spheres is then $4(1-\phi)R/3\phi \approx 0.76R$ which is the length for steps outside the sphere $\langle l_{ext}\rangle$. The distribution of the step lengths outside the spheres should follow the interstice radius distribution of sphere packing [13] and is found nearly exponential at large step lengths. The steps inside the spheres may not be longer than $2R$, and

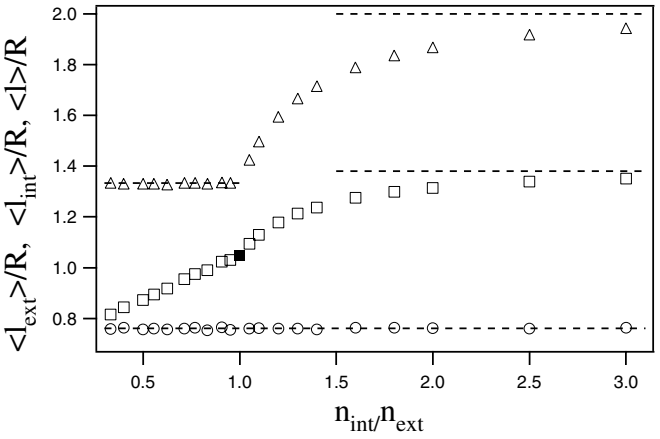

Fig. 1. Steps lengths for a ray propagating through the bead assembly as a function of the refractive index ratio. ∘ are steps lengths for steps outside spheres $\langle l_{ext}\rangle$, △ are lengths for steps inside the spheres $\langle l_{int}\rangle$, and □ are the averaged steps lengths $\langle l\rangle$. Dashed lines and solid symbols are expected limiting behavior for a close packing of spheres as explained in the text.

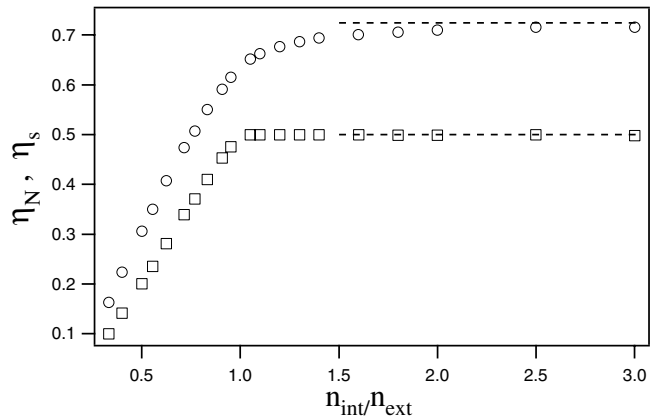

Fig. 2. Fraction η_N of number of steps inside the spheres (□) and fraction of length η_s of the ray inside the spheres (∘) as a function of the refractive index ratio. Dashed lines are the expected limiting behavior for a close packing of spheres.

their length distribution and mean length depend on the refractive index ratio. If $n_{int} < n_{ext}$, the optical rays penetrating the spheres may have any orientations with respect to the normal, and thus the lengths l_{int} are distributed between 0 and $2R$ with a distribution $P(l_{int}) = l_{int}/(2R)^2$ and then $\langle l_{int}\rangle = 4R/3$. If $n_{int} > n_{ext}$, the rays inside the spheres are not allowed to make angles greater than $\arcsin(n_{ext}/n_{int})$, thus increasing the mean lengths for steps inside the spheres. In the limit $n_{int} \gg n_{ext}$, steps inside the spheres are near the spheres diameters, and the mean length of steps is then $\langle l_{int}\rangle = 2R$.

The number of steps inside and outside the spheres are not the same. In Figure 2 the fraction of steps inside the spheres is plotted:

$$\eta_N = \frac{N_{int}}{N_{int} + N_{ext}}\,, \tag{2}$$

where N_{int} (respectively, N_{ext}) is the number of steps inside spheres (respectively, outside) as a function of the refractive index ratio. For $n_{int} < n_{ext}$, the possibility of total refraction favors outside paths. This cannot occur for $n_{int} > n_{ext}$, since the incident angle of a ray impacting a sphere should be the same as the angle of the ray emerging from the sphere, whatever the number of internal reflections. It follows from the symmetry of the Fresnel formulas that the number of paths inside and outside the sphere should be $\eta_N = 1/2$.

For a given ray

$$\eta_s = \frac{N_{int}\langle l_{int}\rangle}{N_{int}\langle l_{int}\rangle + N_{ext}\langle l_{ext}\rangle} \tag{3}$$

is the fraction of the length of the ray which is outside the spheres and is also plotted in Figure 2. If $m = 1$, this fraction is evidently ϕ, and in the limit $n_{int} \gg n_{ext}$, where $\langle l_{int}\rangle = 2R$, we obtain $\eta_s = 3\phi/(2+\phi) \approx 0.73$. It should be stressed that when m decreases, the fraction of the length η_s indicating that the light propagation occurs preferentially outside the spheres. This situation is similar to the propagation of light through the Plateau borders into a dry foam [14,15]. The fraction of length inside or outside the spheres may be also directly measured by considering media with different absorptions, as has been done in an aqueous foam [16].

Finally, the mean step length is defined as

$$\langle l\rangle = \eta_N\langle l_{int}\rangle + (1-\eta_N)\langle l_{ext}\rangle. \tag{4}$$

If $n_{int} = n_{ext}$, rays are straight lines with an equal probability of outside and inside steps, and $\langle l\rangle = 2R/3\phi \approx 1.05$. If $n_{int} \gg n_{ext}$ the average mean free path should be $R(2+\phi)/(3\phi) \approx 1.38R$.

2.3 Transport mean free path

A ray propagating in the beads packing follows a persistent random walk governed by a succession of reflections and refractions. For a large number of scattering events, this random walk may be described by a diffusion process with a diffusion coefficient D, or by the transport mean free path l^* defined as $D = vl^*/3$, where v is the speed of light through the bead packing. The diffusion coefficient is defined by requiring that the mean square displacement $\langle L_s^2\rangle$ between two points separated by a distance s along the ray should be $6Ds/v$ for long enough distance s [17]. This, with the definition of l^* leads to

$$l^* = \lim_{s\to\infty} \frac{\langle L_s^2\rangle}{2s}. \tag{5}$$

For every refractive index ratio, a ray with 10^6 scattering events is computed, $\langle L_s^2\rangle$ is computed by a moving averaging along the ray, and l^* is determined using a linear fit of (5) at large values of s. It has been checked that the determined values are in agreement with a numerical experiment where the transmittance of a slab as a function of its thickness is measured and compared to theoretical expressions [18]. The results are summarized in Figure 3.

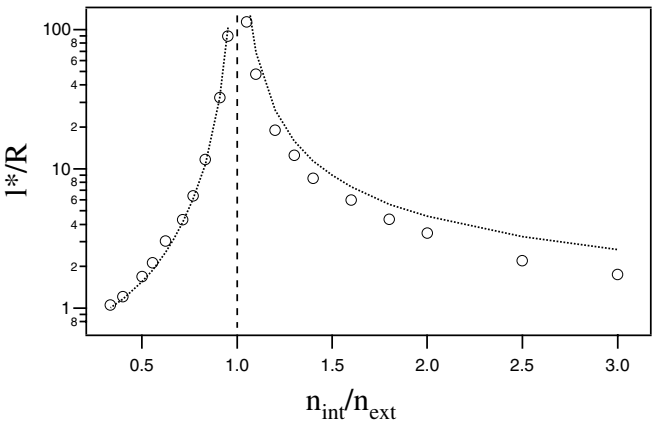

Fig. 3. Transport mean free path as a function of the refractive index ratio (○). The dotted line is $\langle l\rangle/(1-g)$. The dashed line is the asymptote at $n_{int} = n_{ext}$.

The transport mean free path diverges at $n_{ext} = n_{int}$ and decreases to non-trivial values for large or small ratio of refractive index. If the scattering events are independent, it is well known that $l^* = l/(1-g)$, where $g = \langle\cos(\theta)\rangle$ is the average of the cosine of the scattering angle. The computed value of $l/(1-g)$ is plotted in Figure 3. The difference at large values of the ratio of refractive indexes proves that the scattering events are not independent in this limit. Indeed, in this limit, rays may be trapped in a sphere and suffer a succession of scattering event with the same scattering angle and in the same scattering plane. The effect of such correlated scattering events is to slow down the diffusive transport of light, and then to lower the transport mean free path with respect to the case of non-correlated scattering events.

The transport mean free path is typically of the order of a few mean free paths, indicating that a few scattering events are necessary in order to randomize the ray orientation. These trends are similar to light propagation in a dry foam [19,14]. For practical uses, the following numerical expressions may be used for l^* as a function of the refractive indexes ratio $m = n_{int}/n_{ext}$: $l^* = R/(-0.33782 + 0.34122m - 0.01368m^2)$ for $1.05 < m < 3.0$ and $l^* = R/(2.3843 - 4.6267m + 2.2416m^2)$ for $0.33 < m < 0.95$ with a maximum relative error of 6%. For glass spheres $n = 1.52$, $l^* = 6.65R$ if the spheres are dispersed in air, and $l^* = 34R$ if they are dispersed in water.

We now compare these results with some reported values of l^*. Considering the granular "gaseous" flow of granular media in a vertical pipe, Menon *et al.* [4] determined $l^* \approx 15R$ for glass spheres of radius 47 μm dispersed in air. This measure was done by comparison of the time decay of the Diffusing Wave Spectroscopy in different geometries. The variation of the density in the flow compared to the close-packing density is expected to be totally negligible compared to common experimental errors. The optical properties of glass beads dispersed in water have been investigated by Leutz *et al.* [20]. They found l^* ranging from

$14R$ to $16R$ depending on the optical wavelength for beads of radius between 80 μm to 200 μm. Those measures have been done by analyzing the variation of the optical transmission of a slab as a function of its thickness. Those two reported measurements led to the same ratio l^*/R, despite the variation of the dispersing phase. This fact is in disagreement with a visual inspection of glass spheres in air and in water which look different to the human eye, and with a rapid check of the transmitted light across a slab.

3 Deformation of the spheres packing

3.1 Dynamic light scattering

We are now interested in the study of the deformation of the packing of spheres. In light scattering experiments, the motion of the scatterers is probed by monitoring the time autocorrelation function $g_E(t_1,t_2) = \langle E(t_1)E^*(t_2)\rangle/\langle|E(t_1)|\rangle\langle|E(t_2)|\rangle$, where $E(t)$ is the scattered electric field, t_1 and t_2 are two different times, and $\langle\ldots\rangle$ corresponds to averages over many speckle spots [21–23]. Within the weak-scattering limit ($\lambda \ll l$), and in the multiple-scattering regime ($L \gg l$, where L is the dimension of the sample cell), $g_E(t_1,t_2)$ may be expressed as [24,25]

$$g_E(t_1,t_2) = \int_s P(s)\langle \exp^{j\Delta\Phi_s(t_1,t_2)}\rangle \mathrm{d}s, \qquad (6)$$

where $\Delta\Phi_s(t_1,t_2)$ is the phase difference of an optical path of length s between the times t_1 and t_2 and contains the information about the motion of the scatterers; $\langle\ldots\rangle$ is an average on all paths of length s, and $P(s)$ is the path length distribution, and depends on the transport mean free path and on the geometry of the experiment. Be a scattering sequence for a photon within the packing of spheres as shown in Figure 4. We consider a piece of path joining two points $\mathbf{r}_\nu$ and $\mathbf{r}_{\nu+2}$. In the geometrical optic limit, among all the possible paths joining those two points, only paths which are near the ray computed according to the Snell-Descartes laws must be considered in order to compute the electric field scattered from $\mathbf{r}_\nu$ at point $\mathbf{r}_{\nu+2}$. Indeed the interferences of the scattered waves from all the possible paths cancels, except in the vicinity of the geometrical optic ray whose optical path length is stationary. The distance between successive scattering events being of order $\sim R$, the extension of the zone around the geometrical optic ray which contributes to the scattered field is of order $\sim \sqrt{\lambda_0 R}$, with λ_0 the vacuum wavelength. As long as the displacements of spheres are small compared to this extension, and since the wavelength λ_0 is negligible compared to the distance between scattering events R, we may calculate the variation of the phase due to the displacement of the point $\mathbf{r}_{\nu+1}$ as if this point is lightened by a plane wave. In practice, the displacements of the scattering points measured with Diffusive Wave Scattering are $\sim \lambda_0/\sqrt{N}$, where N is the number of scattering events. Since $\sqrt{N} \gg 1$ in the multiple-scattering limit and $\lambda_0 \ll \sqrt{\lambda_0 R}$ in the geometrical optic limit, this condition is always fulfilled.

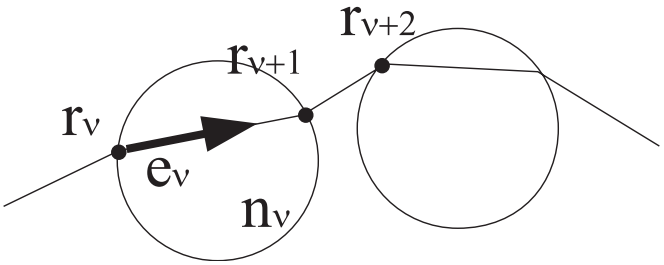

Fig. 4. A scattering sequence of a photon within the packing of spheres.

The phase shift of a N times scattered photon is then

$$\phi_s = k_0 \sum_{\nu=1}^{N} n_\nu |\mathbf{r}_{\nu+1} - \mathbf{r}_\nu|, \qquad (7)$$

where the points $\mathbf{r}_\nu$ are on the rays computed according to the Snell-Descartes Law, n_ν is the refractive index corresponding to the piece of ray between $\mathbf{r}_\nu$ and $\mathbf{r}_{\nu+1}$ and $k_0 = 2\pi/\lambda_0$.

3.2 Deformation of the granular material

We now consider a deformation of a sphere packing between times t_1 and t_2. Many different kinds of deformations may be considered depending on the mechanical properties of the spheres, on the surrounding medium, and on the deformation field within the material. In this study, we restrict ourselves to a totally affine displacement field, which corresponds to the case where the spheres and the continuous media are deformed identically. Such a situation may correspond to experiments where air bubbles are trapped within a gel which is sheared. This simplification of the deformation field does not take into account some possible non-deterministic motions of the scatterers as may occur if the material is submitted to mechanical vibrations, or possible deviations to affine displacement field as it could occur in deformed granular media.

With this hypothesis, the problem is closely related to the problem of the fluctuation of the intensity scattered by a colloidal suspension submitted to a shear flow, which has been investigated in details by Bicout *et al.* [26–28]. If the deformation field varies slowly at the scale of the mean free path, the variation of the phase given by equation (7) between times t_1 and t_2 may be expressed as [27]

$$\Delta\Phi_s(t_1,t_2) = k_0 \sum_{\nu=1}^{N} \sum_{i,j} n_\nu l_\nu e_{\nu,i} e_{\nu,j} U_{ij}\,, \qquad (8)$$

where $l_\nu = |\mathbf{r}_{\nu+1} - \mathbf{r}_\nu|$, $e_{\nu,i}$ is the component along direction i of the unitary vector $\mathbf{e}_\nu$, and $U_{ij} = (1/2)(\partial U_i/\partial x_j + \partial U_j/\partial x_i)$ is the deformation tensor. For needs of simplicity, in the following we will drop the references to the times t_1 and t_2, and simply write $\Delta\Phi_s$

The phase variation involved in equation (7) is the sum on a large amount of individual phase variations, and thus

is a random Gaussian variable. It follows from the central-limit theorem that the average phase factor involved in equation (6) is

$$\langle \exp^{j\Delta\Phi_s} \rangle = \exp^{j\langle\Delta\Phi_s\rangle} \exp^{-(\langle\Delta\Phi_s^2\rangle - \langle\Delta\Phi_s\rangle^2)/2} . \quad (9)$$

The average phase variation may be calculated as [26]

$$\begin{aligned}\langle\Delta\Phi_s\rangle &= k_0 N \langle l_\nu n_\nu\rangle \langle e_{\nu,i} e_{\nu,j}\rangle U_{ij} \\ &= \frac{1}{3} k_0 s \langle n\rangle \sum_i U_{ii} \,, \end{aligned} \quad (10)$$

where $\langle n\rangle = \langle n_\nu l_\nu\rangle / \langle l_\nu\rangle$. As pointed out by Bicout in the study of flows of colloidal suspensions by Diffusive Light Scattering [26], variations of the mean phase shifts are associated with the variations of the volume of the material. The evaluation of the mean square of the phase variation,

$$\begin{aligned}\langle\Delta\Phi_s^2\rangle = k_0^2 \Bigg\langle & \sum_{\nu,\nu'=1}^{N} l_\nu l_{\nu'} n_\nu n_{\nu'} \\ & \times \sum_{i,j,k,l} e_{\nu,i} e_{\nu,j} e_{\nu',k} e_{\nu',l} U_{ij} U_{kl} \Bigg\rangle, \end{aligned} \quad (11)$$

involves both geometric quantities which depend on the disorder inside the system, and quantities depending on the optical properties through the persistence of the ray orientation across the interface. We first notice that the variance of the phase shift should vary quadratically with the elements of the deformation tensor. In addition the orientation of the rays being isotropic, the variance should depend on the isotropic invariants of the deformation tensor: $(\sum_i U_{ii})^2$ and $(\sum_{i,j} U_{ij}^2)$. Moreover, since the light is multiply scattered, the phase shift is due to a large number of scattering events. It follows that the variation of the phase shift should vary linearly with the number N of scattering events, as well as linearly with the path length s. Taking into account these different remarks, we may postulate that the variance of the phase shift could be written as

$$\begin{aligned}\langle\Delta\Phi_s^2\rangle - \langle\Delta\Phi_s\rangle^2 = k_0^2 s \\ \left((\beta - \chi) \left(\sum_i U_{ii} \right)^2 + 2\beta \sum_{i,j} U_{ij}^2 \right), \end{aligned} \quad (12)$$

where β and χ are two lengths which depend on the geometric characteristic of the rays, and which scale as the bead radius.

The analytical form (12) for the variance of the phase shift has been checked numerically by computing the phase variation of rays of different path lengths s, after deformation of different amplitudes and due to different deformation tensors. Figure 5 shows the variations of the two lengths β and χ with respect to the ratio between the two refractive indexes as determined by the numerical algorithm. Those lengths diverge at $n_{ext} = n_{int}$ and show non-trivial variations as the mismatch between the indexes of spheres and surrounding medium increases.

3.3 Approximate expressions

Further analytical computations of β and χ require more knowledge of the correlations along a geometric ray, such as the correlations between the orientations of the successive rays or correlations between orientations and length.

Such a computation has been derived by Bicout *et al.* [28] for colloidal suspensions where there are no correlations of the lengths between successive scattering events, where the path lengths between two scattering events are distributed along a negative exponential function, and where the variations of the orientations along rays are given by Mie scattering. Under these hypotheses, they found the expression (12), with a value of $\beta = 2l^*/15$. The value of χ has not been computed since they consider only incompressible deformations of fluid.

The result of this model is shown as the plain line in Figure 5, and reproduces qualitatively well the numerically observed behavior, *i.e.* the divergence close to the matching between spheres and surrounding media, with a reasonable quantitative agreement. However this model is unable to take into account the numerically observed behavior as the mismatch between spheres and surrounding media increases. Those differences should be taken into account in a more complex model which would consider not only the correlations between the orientations of the segments along the rays, but also the correlations between the scattering angles along the rays. Such correlations are expected to arise from successive correlated scattering events, as it could occur when a ray is trapped within a sphere and then suffers well-correlated scattering events. However, from an experimental point of view, those effects are of minor importance if the ratio of refractive indexes is kept in the range 0.7–1.5, as is the case for common liquid foams, emulsions, or glass beads dispersed in water or glass.

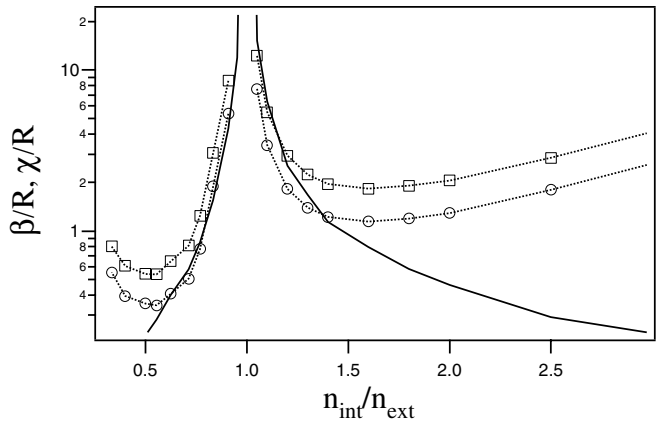

Fig. 5. Variation of the lengths β (○) and χ (□) with the refractive index ratio. Dotted lines are for guidelines. Plain lines: values of β expected from reference [28].

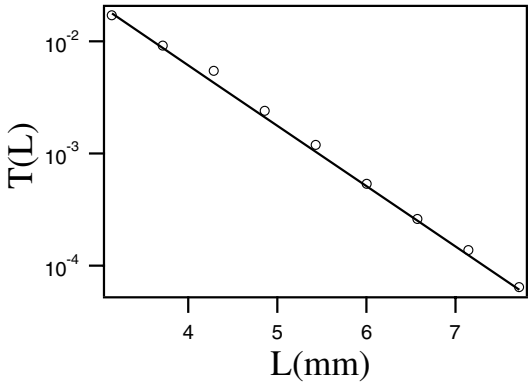

Fig. 6. Transmission of glass beads packing as a function of the thickness cell (○). Plain line: best fit according to equation (13).

4 An Experimental test

4.1 Experimental set-up

The preceding discussions and developments rely on the hypothesis that the propagation of the light within the beads packing may be described within the geometrical optics framework, and that Diffusing Wave Spectroscopy experiment may be understood within this framework. We propose now a static and a dynamic light scattering on a glass bead packing dispersed in air. Experiments are performed with Silibeads®Soda-Lime glass spheres from Sigmund Lindner GmbH. Beads radius are selected by sieving in a range of radius $R = 35\,\mu$m to $R = 45\,\mu$m. Particles are then washed with water in order to remove possible dusts, and then dried. A microscopic inspection of the particles shows that broken beads or clearly elliptical shaped beads are present and represent typically 10% of the beads.

4.2 Transmission experiments

The transport mean free path is determined by measuring the light transmission ratio of beads packing as a function of its thickness. For this we disposed the beads in a dihedral cell whose thickness varies from $L = 2\,$mm to $L = 10\,$mm, and with an aperture angle $\alpha \approx 60\,$mrad. The cell is illuminated with a stabilized $633\,\mu$m laser (Melles Griot 05STP903), and the scattered light is collected with microscope objective and focussed on a silicon photodiode. The transmissivities are normalize with the diffuse intensity transmitted through a reference polyball sample (monodisperse polystyrene spheres of size $0.73\,\mu$m, thickness of sample 3.1 mm, volume fraction $\phi = 0.64\%$, transport mean free path $430\,\mu$m).

Figure 6 shows the evolution of the transmission as a function of the cell thickness. Data are fitted according to [20]

$$T(L) = \frac{l^*}{L_a} 2(\beta+\gamma) \frac{1}{1+2\beta l^*/L_a} \exp -(L/L_a), \qquad (13)$$

where L_a is the absorption length, γ is the distance expressed in l^* from the boundary at which the diffusion approximation is valid, and which is taken as unity, and $\beta = (2/3)(1+R)/(1-R)$ is the reflection coefficient of the diffusing wave, with R the reflection coefficient of the air/glass/air interface. Best fits leads to $L_a = 805 \pm 20\,\mu$m and $l^* = 330 \pm 40\,\mu$m, in reasonable agreement with the value $l^* = 266\,\mu$m expected from the ray tracing approach.

4.3 Diffusing Wave Spectroscopy experiment

There is, to the knowledge of the author, no clear way to produce a well-know displacement field within a granular medium. This is due to the nature of the dry solid contact which may produce different deviations to affine deformation field, including plastic events. As a consequence, there is no simple equivalent to Brownian colloidal particles in order to test Diffusing Wave Spectroscopy for affine deformation field within solid granular matter.

We propose however to examine and analyze the thermal dilatation of a granular beads within the optical geometric framework. Experiments are performed with the same soda lime glass beads which are contained in optical glass spectrometry cell of thickness $L = 5.0\,$mm. The optical cell is enclosed in a temperature controlled cell whose temperature is controlled with a stability of few mK [29]. The material is lightened with the non-extended laser beam, and the scattered transmitted light is collected through a 3 mm diameter diaphragm aligned with the incident beam. The scattered light is then recorded at a frame rate of 1 Hz with a 8bit monochrome camera (Cohu 4910). The speckle size is fixed to 3 pixels and $\sim 4 \cdot 10^4$ speckle spots are recorded simultaneously. The experimental contrast of the scattered intensity $\langle I^2\rangle/\langle I\rangle^2$ is typically 0.3. The temperature of the granular material is varied at the rate $0.01\,^\circ$C/mn around a mean temperature of $32\,^\circ$C, and the evolution of the scattered light is measured during those variations. It as been checked that variations of a factor two of the cooling or heating rate does not have visible effects on the experimental results. The correlation of the scattered intensities are measured as

$$g_I(T_1,T_2) = \frac{\langle I_p(T_1) I_p(T_2)\rangle}{\langle I_p(T_1)\rangle\langle I_p(T_2)\rangle} - 1, \qquad (14)$$

where $I_p(T)$ is the intensity recorded at temperature T on the pixel p, and $\langle\ldots\rangle$ corresponds to an average over the pixels of the camera. Data are corrected from experimental noise and normalized with a procedure described elsewhere [30].

The plain line in Figure 7 is a plot of the correlation as a function of the temperature difference. The experimental results are now compared with the numerical results of the ray-tracing algorithm. In order to do this, we first compute a large number M of rays propagating through the sample. Then, for each ray m, the variation of the phase shift $\Delta\Phi^{(m)}$ due to the dilatation is calculated from equation (10) assuming that the deformation tensor is $U_{ij} = \delta_{ij}\alpha\Delta T$ as

$$\Delta\Phi^{(m)} = k_o s \langle n\rangle \alpha \Delta T. \qquad (15)$$

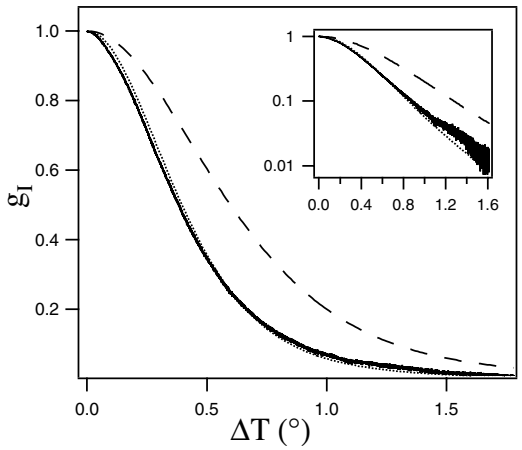

Fig. 7. Plain line: measured intensity correlation as a function of the glass beads temperature difference. Dashed line: intensity correlation function computed from the optical geometric model assuming a uniform dilatation coefficient of $\alpha = 8.6 \cdot 10^{-6}\,\mathrm{K}^{-1}$. Dotted line: computed intensity correlation function for a glass sphere packing of average radius for a uniform dilatation coefficient of $\alpha = 12 \cdot 10^{-6}\,\mathrm{K}^{-1}$.

In deriving equation (15) we have neglected the variation of the refractive index of the glass with the temperature. This assumption is justified by the fact that at the experiment temperature, the thermo-optical effect for Soda Lime glass $(1/n)(\partial n/\partial T) \approx -1.3 \cdot 10^{-6}\,\mathrm{K}^{-1}$ [31] is small compared to dilatation effect $\alpha \approx 8.6 \cdot 10^{-6}\,\mathrm{K}^{-1}$. Equation (15) simply states that under a thermal isotropic dilatation, a path of length s is dilated of $\alpha \Delta T s$, whatever the geometrical aspect of this path.

The normalized correlation function of the scattered electric field g_E is then computed as

$$g_E = \frac{\sum_{m=1}^{M} \exp(j\Delta\Phi^{(m)}) \exp(-s/l_a)}{\sum_{m=1}^{M} \exp(-s/l_a)} \qquad (16)$$

with $l_a = 3L_a^2/l^*$ [16,18]. The exponential damping factor takes into account the absorption measured in Section 4.2. The normalized correlation function of the scattering intensity is then computed using the Siegert relation,

$$g_I = |g_E|^2 . \qquad (17)$$

The dashed lines in Figure 7 is a plot of the computed intensity correlation function for the packing of spheres with the geometrical parameters $R = 40\,\mu\mathrm{m}$, $L = 5\,\mathrm{mm}$, $L_a = 805\,\mu\mathrm{m}$ according to Section 4.2 and $\alpha = 8.6 \cdot 10^{-6}\,\mathrm{K}^{-1}$. This evidences that this optical geometric model is able to take into account the deformation of the sphere packing. The discrepancy between the measurement and the prediction of the optical geometric model may be due to numerous simplifying assumptions as the use of monodisperse spheres or strictly affine displacement field, and separated studies should be necessary in order to take into account such effects. It should be stressed that the computed correlation function is very sensitive to the experimental parameters, and especially to the deformation of the sphere packing. The dotted line in Figure 7 is a plot of the computed correlation function with the same parameter set, except the dilatation coefficient which is taken to $\alpha = 12 \cdot 10^{-6}\,\mathrm{K}^{-1}$. It appears very plausible that deformation field is not only composed of a strictly affine one, but also a non-affine deformation takes place, which could explain an increased of the net displacement compared to the expected one.

5 Conclusion

We developed a ray-tracing program in order to simulate the propagation of the light through a random close packing of dielectric spheres. This allowed us to compute the geometrical quantities associated with the random walk of the optical ray through the sample. The effects of the deformations of the materials may be taken into account by considering the variance of the variations of the phase shifts during the motion of particles. The results are found to be very similar to the problem of the deformation of a colloidal suspension into a shearing flow. There are however visible effects due to the correlations of the scattering events which are not present inside colloidal suspension. Finally, we performed an experiment on a homogeneous deformation of the materials, and the results were found to be in agreement with the description of geometrical rays propagating through the sample. Different experiments may be considered to test in more details the optical geometric limit of light propagation. The first one should be systematic measurement of the transport mean free path as a function of the ratio of the refractive indexes. This could be done with the measure of the transmitted or backscattered intensities, a method which does not rely on hypotheses on the variations of the phase shifts during the motion of the particles. By considering slightly absorbing glass spheres of interstitial liquid, the predictions on the relative amount of rays within the continuous phase or the spheres should be also testable. The difficulty of deforming a granular medium in a controllable way makes experimental tests about the variations of the phase shifts under deformation difficult. We have in this paper measured the dilatation of granular materials. Another possibility should be to use a sheared wet foam or an emulsion [32]. At large mismatch between the two phases, the effects of internal refractions should be visible, as we may check in Figure 5: at $n_{int}/n_{ext} \approx 2$ there is a factor 5 between predictions which neglect correlations of scattering events compared to more accurate predictions. Finally, from an experimental point of view, Diffusive Wave Spectroscopy appears as a useful method in order to study deformations of granular materials.

I am grateful to C. Baravian for valuable discussions. This work has been supported by ANR grant NT05-4_42012 “MICMAC”.

References

1. R. Garcia-Rojo, H.J. Hermann, S. MacNamara (Editors), *Powder and Grains 2005* (Taylor & Francis Group, London, 2005).
2. X. Jia, C. Caroli, B. Velicky, Phys. Rev. Lett. **82**, 1863 (1999).
3. M.L. Cowan, I.P. Jones, J.H. Page, D.A. Weitz, Phys. Rev. E **65**, 066605 (2002).
4. N. Menon, D.J. Durian, Science **275**, 1920 (1997).
5. K. Kim, J.J. Park, J.K. Moon, H.K. Kim, H.K. Pak, J. Korean Phys. Soc. **40**, 983 (2002).
6. A. Kabla, G. Debrégeas, Phys. Rev. Lett. **92**, 035501 (2004).
7. P.K. Dixon, D.J. Durian, Phys. Rev. Lett. **90**, 184302 (2003).
8. N. Menon, D.J. Durian, Phys. Rev. Lett. **79**, 3407 (1997).
9. W.S. Jodrey, E.M. Tory, Phys. Rev. E **32**, 2347 (1985).
10. H.J. Hoffmann, Appl. Phys. B **70**, 853 (2000).
11. H.J. Hoffmann, Glass Sci. Technol. **76**, 285 (2003).
12. H.C. van de Hulst, *Light Scattering by Small Particles* (Dover, New York, 1957).
13. J.L. Finney, in *Physics of Granular Media*, edited by D. Bideau, J. Dodds (Nova Science Publishers, New York, 1991).
14. M.F. Miri, H. Stark, Europhys. Lett. **65**, 567 (2004).
15. M. Schmiedeberg, M.F. Miri, H. Stark, Eur. Phys. J. E **18**, 123 (2005).
16. A.S. Gittings, R. Bandyopadhyay, D.J. Durian, Europhys. Lett. **65**, 414 (2004).
17. J. Rička, in *Neutrons, X-rays and Lights*, edited by P. Lindner, Th. Zemb (Elsevier, 2002).
18. J.H. Li, A.A. Lisyanski, T.D. Cheung, D. Livdan, A.Z. Genack, Europhys. Lett. **22**, 675 (1993).
19. M.U. Vera, A. Saint-Jalmes, D.J. Durian, Appl. Opt. **40**, 4210 (2001).
20. W. Leutz, J. Rička, Opt. Commun. **126**, 260 (1996).
21. B.J. Berne, R. Pecora, *Dynamic Light Scattering: With Applications to Chemistry, Biology, and Physics* (Wiley, New York, 1976).
22. V. Viasnoff, F. Lequeux, D.J. Pine, Rev. Sci. Instrum. **73**, 2336 (2002).
23. L. Cipelletti, D.A. Weitz, Rev. Sci. Instrum. **70**, 3214 (1999).
24. G. Maret, P.E. Wolf, Z. Phys. B **65**, 409 (1987).
25. D.J. Pine, D.A. Weitz, P.E. Wolf, G. Maret, E. Herbolzheimer, P.M. Chaikin, in *Scattering and Localization of Classical Waves in Random Media*, edited by P. Sheng (World Scientific, 1990).
26. D. Bicout, E. Akkermans, R. Maynard, J. Phys. I **1**, 471 (1991).
27. D. Bicout, R. Maynard, Physica A **199**, 387 (1993).
28. D. Bicout, G. Maret, Physica A **210**, 87 (1994).
29. I. Flammer, G. Bucher, J. Rička, J. Opt. Soc. Am. A **15**, 2066 (1988).
30. L. Djaoui, J. Crassous, Granwar Matter **7**, 185 (2005).
31. N.G.V. Astrath, J.H. Rohling, A.N. Medina, A.C. Bento, M.L. Baesso, C. Jacinto, T. Catunda, S.M. Lima, F.G. Gandra, M.J.V. Bell, V. Anjos, Phys. Rev. B **71**, 214202 (2005).
32. P. Hebraud, F. Lequeux, J.P. Munch, D.J. Pine, Phys. Rev. Lett. **78**, 4657 (1997).